III International Conference on Particle-based Methods – Fundamentals and Applications
PARTICLES 2013
M. Bischoff, E. Oñate, D.R.J. Owen, E. Ramm & P. Wriggers (Eds)

ABSORBING BOUNDARY CONDITIONS FOR GRANULAR ACOUSTICS

SEAN C. MCNAMARA

Université de Rennes 1
Institut de Physique de Rennes - UMR CNRS 6251
Campus de Beaulieu
35042 Rennes Cedex FRANCE
sean.mcnamara@univ-rennes1.fr

Key words: Granular Materials, DEM, Acoustics, Attenuation, Boundary Conditions

Abstract. The boundary conditions of soft-sphere DEM are usually perfect reflectors of acoustic waves, leading to an unrealistic accumulation of energy. This situation is usually dealt with by global damping. In some situations, this solution is undesirable, so we present an alternative. If the grain-wall contact is made soft and dissipative, most acoustic energy incident on the boundary will be trapped and dissipated there. We show that these boundary conditions can efficiently damp both high and low frequency waves.

1 INTRODUCTION

1.1 Motivation

In DEM simulations, the numerical domain is usually bounded by periodic boundary conditions, or fixed or movable walls. These boundary conditions are all nearly perfect reflectors of acoustic waves. In contrast, in experimental or natural settings, a large part of the acoustic energy can usually escape into the environment. This means that acoustic energy is usually trapped unrealistically in granular simulations. This problem is usually dealt with by global damping [1]: a viscous-like force, proportional and opposed to the particle velocity, is applied to each grain, and efficiently removes energy from the system.

Global damping is often effective solution to this problem. But if we wish to study granular acoustics numerically, it has the disadvantage of artificially attenuating waves as they travel through the system. This is why pioneering simulations of granular acoustics [4] concerned quasi-one-dimensional systems that allow one to postpone boundary interactions for a long time. But if one wishes to study more complex systems, such as acoustic emission by destabilized granular material [6] or interactions between acoustic waves and shear bands [7], another solution is needed.

How is this problem solved in related fields? Experimentally, one can isolate an experiment acoustically by layer of some soft, absorbing material. Numerically, when solving

the wave equation, sophisticated boundary conditions exist that can absorb almost all the energy incident on boundaries. As we will see, the solution proposed in this paper resembles both of these examples.

1.2 Organization

This paper is structured as follows. Sec. 2 sketches boundary conditions used in numerical studies of waves in continua. Sec. 3 describes the numerical simulations used in this paper. Sec. 4 describes long-lived free oscillations present in simulated granular packings. This oscillations are a consequence of the energy-conserving boundary conditions. Sec. 5 presents a one-dimensional model of the (two-dimensional) packings that is analytically accessible, yielding a theoretical prediction for the decay of the free oscillations. Sec. 6 presents a highly dissipative boundary condition, and Sec. 7 shows that it effectively absorbs sound waves.

2 BOUNDARY CONDITIONS FOR WAVES IN CONTINUA

The most effective absorbing boundary condition for waves in numerical continuum studies are "perfectly matched layers". They were first introduced for electromagnetic waves [2]. They have since been modified and adapted to acoustic waves [3]. But the original reference [2] gives a clearer physical picture, and we therefore sketch the proposed method in this section.

Ref. [2] begins by considering transverse electric waves, where the electric field is in the plane of propagation. Acoustic waves obey the same equations, as one can see by simply renaming variables:

$$\epsilon_0 \frac{\partial E_x}{\partial t} + \sigma E_x = \frac{\partial H_z}{\partial y} \quad \Rightarrow \quad \rho_0 \frac{\partial u_y}{\partial t} + \sigma u_y = -\frac{\partial p}{\partial y}, \tag{1a}$$

$$\varepsilon_0 \frac{\partial E_y}{\partial t} + \sigma E_y = -\frac{\partial H_z}{\partial x} \quad \Rightarrow \quad \rho_0 \frac{\partial u_x}{\partial t} + \sigma u_x = -\frac{\partial p}{\partial x}, \tag{1b}$$

$$\mu_0 \frac{\partial H_z}{\partial t} + \sigma^* H_z = \frac{\partial E_x}{\partial y} - \frac{\partial E_y}{\partial x} \quad \Rightarrow \quad \frac{1}{\rho_0 c^2}\frac{\partial p}{\partial t} + \sigma^* p = \frac{\partial u_x}{\partial x} + \frac{\partial u_y}{\partial y}. \tag{1c}$$

On the left, we have written the electromagnetic wave equations [2], and on the right, the equations describing acoustic waves in a fluid with density ρ_0, pressure p_0, and a linearized equation of state $p = c^2(\rho - \rho_0) + p_0$. The acoustic equations are obtained from the electromagnetic ones by the substitution $\epsilon_0 \to \rho_0$, $\mu_0 \to 1/\rho_0 c^2$, $E_x \to u_y$, $E_y \to -u_x$, $H_z \to -p$. The constants σ and σ^* provoke the decay of waves. In the electromagnetic case, they are conductivities, and in empty space, $\sigma = \sigma^* = 0$.

One way to implement an absorbing boundary is to set $\sigma \neq 0$, $\sigma^* \neq 0$ in a narrow strip next to the boundaries. To avoid reflections at the inner boundary or the strip, the relation $\sigma/\sigma^* = \varepsilon_0/\mu_0 = \rho_0^2 c^2$ is required. Could this boundary condition be implemented in a particle method? Setting $\sigma \neq 0$ is what is done in global damping, but setting $\sigma^* \neq 0$ is not possible, for we do not directly manipulate the stress in particle methods.

In any case, this method has problems because it damps waves traveling parallel to the boundaries in the same way as incident waves, leading to distortion. "Perfectly matched layers" fix this problem. In this method, the pressure field is split into two parts p_x and p_y, where p_x couples to waves propagating in the x-direction, and p_y to y-directed waves. Furthermore, the damping coefficients are also split: $\sigma \to \sigma_x, \sigma_y$, $\sigma^* \to \sigma_x^*, \sigma_y^*$ The wave equations become

$$\rho_0 \frac{\partial u_x}{\partial t} + \sigma_x u_x = -\frac{\partial p_x}{\partial x} - \frac{\partial p_y}{\partial x}, \qquad \frac{1}{\rho_0 c^2}\frac{\partial p_x}{\partial t} + \sigma_x^* p_x = \frac{\partial u_x}{\partial x}, \tag{2a}$$

$$\rho_0 \frac{\partial u_y}{\partial t} + \sigma_y u_y = -\frac{\partial p_x}{\partial y} - \frac{\partial p_y}{\partial y}, \qquad \frac{1}{\rho_0 c^2}\frac{\partial p_y}{\partial t} + \sigma_y^* p_y = \frac{\partial u_y}{\partial y}, \tag{2b}$$

Note that if $\sigma_x = \sigma_y$ and $\sigma_x^* = \sigma_y^*$, then the pressure equations can be added together, leading back to Eq. (1). Thus Eqs. (2) are a generalization of Eqs. (1). Note also that a wave traveling in the x-direction is governed solely by Eq. (2a), while a y-directed wave solely by Eq. (2b). Thus setting $\sigma_x, \sigma_x^* \neq 0$ and $\sigma_y = \sigma_y^* = 0$ leaves y-directed waves unmolested. This cures the remaining problems of Eqs. (1).

The absorbing boundaries proposed in this paper contain two features of the methods presented here:

1. A global-damping-like coefficient that is nonzero only near the boundaries, and
2. Anisotropic damping such that waves propagating parallel to the boundaries are undamped.

3 NUMERICAL SETUP

This section describes the numerical simulations used in this paper. We first discuss the particle interactions, and then the system parameters, such as size, number of particles, etc.

3.1 Particle interactions

We use the very common "Molecular Dynamics" or "Soft-Sphere DEM" method. The forces between the grains are calculated, and Newton's second law is integrated to obtain their motion. With the exception of the rolling torque, we use standard linear contact forces. Even though these forces have been presented many times before, we present a rapid review to define our symbols.

The normal contact force F_n is given by

$$F_n = -K_n D_n - \gamma_n \dot{D}_n, \text{ where } D_n = |\mathbf{x}_i - \mathbf{x}_j| - a_i - a_j. \tag{3}$$

Here, $\mathbf{x}_1$ and $\mathbf{x}_2$ are the grain positions, and a_1 and a_2 are their radii. K_n and γ_n are constants that describe grain stiffness and energy dissipation. We require $F_n \geq 0$, that is, that the normal force be repulsive. If Eq. (3) yields a negative number, we set $F_n = 0$.

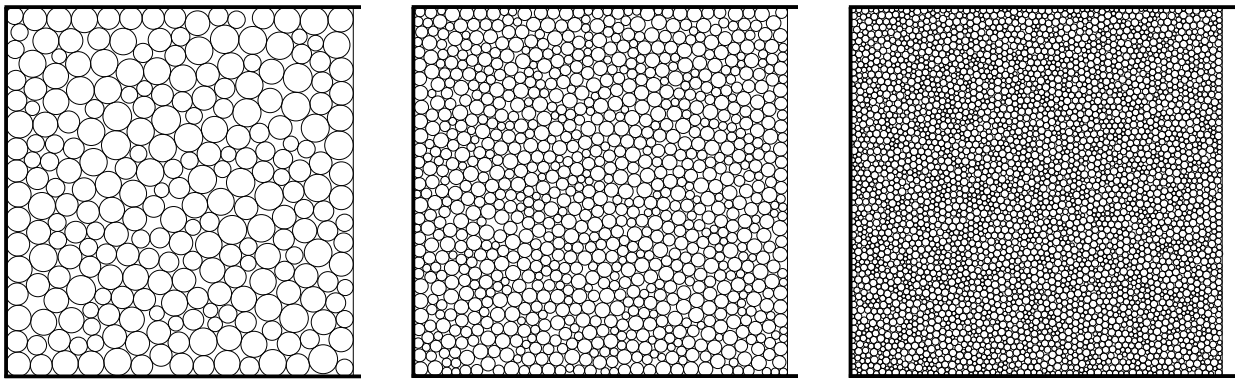

$N = 16 \times 16 = 256$ $N = 32 \times 32 = 1024$ $N = 64 \times 64 = 4096$

Figure 1: Numerical setup: The upper, lower, and left walls are fixed (heavy lines). A constant pressure p_* is applied to the right wall (thin line). We study five "generations" with $N = 256, 1024, 4096, 16384, 65336$ grains. The first three generations are shown above. From one generation to the next, N is multiplied by four.

A tangential interaction force F_t is implemented in an analogous way:

$$F_t = -K_t D_t - \gamma_t \dot{D}_t, \text{ where } \dot{D}_t = -a_i\omega_i - a_j\omega_j + (\mathbf{v}_i - \mathbf{v}_j)\cdot\mathbf{t}, \tag{4}$$

where ω_i and ω_j are the angular velocities of the touching particles, and $\mathbf{t}$ is a unit vector tangent to the particle surfaces at the point of contact. K_t, γ_t are analogous to K_n, γ_n. Note that D_t must be found by integrating the differential equation given above.

The tangential force must obey the Coulomb friction law: $|F_t| \le \mu F_n$, where μ is the friction coefficient. If F_t calculated from Eq. (4) does not satisfy this inequality, F_t is set equal to $\pm\mu F_n$, and D_t is adjusted as well.

In addition to the normal and tangential forces we apply a rolling torque:

$$\tau_r = -a_{12}\left(K_r D_r + \gamma_r \dot{D}_r\right), \text{ where } \dot{D}_r = a_{12}\left(\omega_1 - \omega_2\right). \tag{5}$$

Here $a_{12} = a_1 a_2/(a_1 + a_2)$. Equal and opposite torques of this magnitude are applied to the grains to oppose the rolling motion. The maximum rolling torque is proportional to the normal force: $|\tau_r| \le \mu_r F_n a_{12}$, where μ_r is a dimensionless number analogous to the friction coefficient. If this condition is not satisfied, we set $\tau_r = \pm\mu_r F_n a_{12}$.

3.2 System Description

As shown in Fig. 1, we study two-dimensional packings of N circular grains in two-dimensions confined by four walls. The top, bottom, and left walls are fixed, and the right hand wall is mobile. A fixed pressure p_* is applied to the mobile wall, whose motion is obtained obtained by integrating Newton's second law, as if it were a grain.

We will examine a series of packings of with $N = 256, 1024, 4096, 16384, 65336$ grains. But the total mass of the grains is always the same and equal to M_*. The density of

grains also remains constant and equal to ρ_*. Changing the number of grains, therefore, means that their average radius is divided by 2 every time we multiply N by 4. Some examples of the packings are shown in Fig. 1.

For all simulations, $K_n = 2000p_*$ and $D_n = 0.2\sqrt{K_n M_*/N}$. This choice gives a restitution coefficient of about 0.92, independent of N. The other particle interaction coefficients are proportional to K_n and D_n. In particular, we set $K_t = K_n/2$, $D_t = D_n/2$, $K_r = K_n/10$, and $D_r = D_n/10$. The friction ratios are $\mu = 0.2$ and $\mu_r = 0.02$. The walls are always smooth, i.e. they exert only normal forces.

The quantities p_*, M_*, and ρ_* define the units used throughout this paper. We are working in two-dimensions, so ρ_* has units of mass divided by length squared, and p_* has units of force divided by length. This implies that the unit of length is $\ell_* = \sqrt{M_*/\rho_*}$, the unit of time is $t_* = \sqrt{M_*/p_*}$. The unit of velocity is $v_* = \sqrt{p_*/\rho_*}$, and the unit of energy is $E_* = M_* p_*/\rho_*$.

The initial conditions are obtained by compressing a granular gas. The top and right walls are made mobile, and a pressure p_* is applied. The grains are compressed into a stationary packing.

4 FREE OSCILLATIONS

To illustrate the problem that this paper seeks to solve, we will generate a standing wave inside the packing and examine its decay. The longest lived sound wave is a longitudinal wave oriented in the x-direction, with a wavelength of four times the system length. The x-component of the velocity of grain k is approximately

$$v_k = A \sin\left(\pi x_k/(2L_x)\right), \tag{6}$$

where x_k is the x-coordinate of grain k, A is a wave amplitude, and L_x is the position of the right hand wall. (The left hand wall is at $x = 0$.)

To study the behavior of this wave, we use Eq. (6) with $A = 10^{-4} v_*$ to set the initial velocities of the grains (and the mobile wall). The system then evolves without further injection of energy. Fig. 2 shows the kinetic energy as a function of time for a packing of $N = 32 \times 32 = 1024$ grains. As shown in the figure, the kinetic energy undergoes rapid oscillations of gradually decaying amplitude.

Fig. 2 also shows the envelopes of the energy for systems with different numbers of particles. As one can see, the decay becomes slower and slower as the number of grains increases, in contrast to the period of oscillation that remains almost constant in all simulations.

5 ONE-DIMENSIONAL MODEL

In this section, we study a one-dimensional model that gives an analytic prediction of the oscillation period and decay rate of the free oscillations.

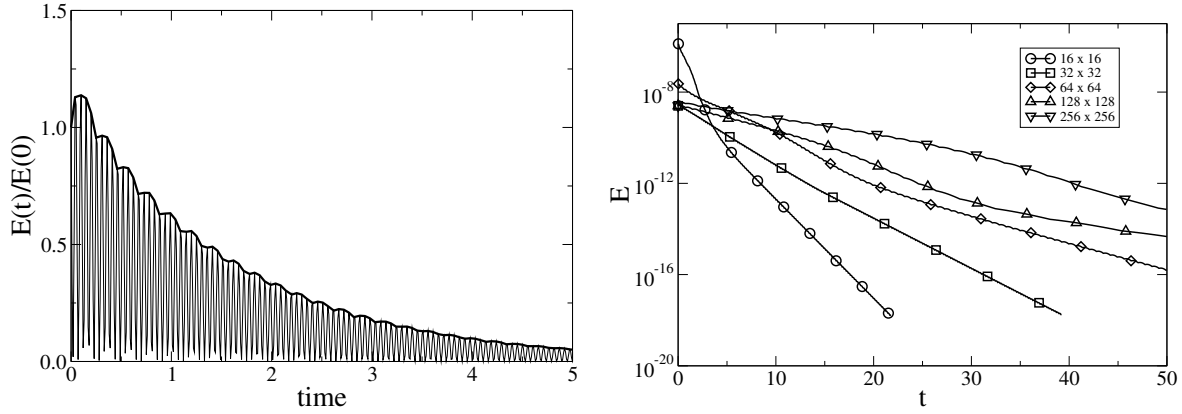

Figure 2: Left: Kinetic energy as a function of time in a simulation of $N = 32 \times 32 = 1024$ grains that has been gently excited according to Eq. (6). The thin line shows the evolution of the energy and the thick line shows the envelope of the oscillations obtained by plotting all the local maxima of the thin line. Right: Energy envelopes for systems of different sizes.

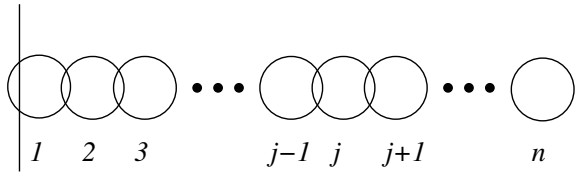

Figure 3: The one-dimensional model of the two-dimensional systems shown in Fig. 1. The wall on the left is fixed. The n grains are always in contact.

5.1 Analytical model

Let us idealize the disordered packings of poly-disperse grains shown in Fig. 1 as square crystalline packings of mono-disperse grains. The crystalline packings consist of a square, $n \times n$ array ($n = \sqrt{N}$) of grains all with mass $\bar{m} = M_*/n^2$. These packings can be considered as n rows containing n grains each, as shown in Fig. 3. The grains interact via Eq. (3), except that attractive forces are allowed. We label the grains $j = 1 \ldots n$, and assume $x_1 < x_2 < \cdots < x_n$, with x_j being the position of grain j. We suppose that grain n free to move. The equation of motion of grain j is [5]

$$\bar{m}\ddot{x}_j = K_n(x_{j+1} - 2x_j + x_{j-1}) + D_n(\dot{x}_{j+1} - 2\dot{x}_j + \dot{x}_{j-1}). \tag{7}$$

We assume a solution of the form

$$x_j(t) = j\Delta x + Ae^{st}e^{i\pi jm/n}, \tag{8}$$

where Δx is the equilibrium separation of neighboring grains, and A, s, and m are parameters to be found. Putting this solution into Eq. (7) and assuming that $n \gg 1$ yields

$$s = -\mu \pm \sqrt{\mu^2 - \omega^2}, \text{ where } \mu = \epsilon^2 \frac{D_n}{2\bar{m}}, \quad \omega = \epsilon\sqrt{\frac{K_n}{\bar{m}}}, \quad \epsilon \approx \frac{\pi m}{n}. \tag{9}$$

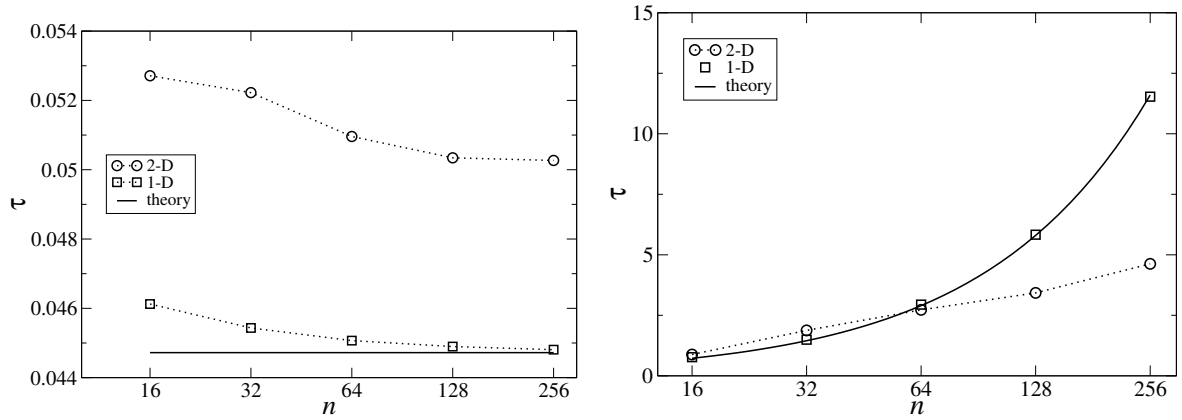

Figure 4: Left: Periods of the kinetic energy oscillations. Right: The characteristic decay time τ, as a function of $n = \sqrt{N}$.

Here, m identifies the harmonic mode being studied. Comparing Eq. (8) and Eq. (6) indicates we should set $m = 1/2$, where n grains corresponds to one quarter wavelength. Setting $\bar{m} = M_*/n^2$ and using the grain-grain interactions described in Sec. 3 leads to

$$\omega = \frac{\pi}{2}\sqrt{\frac{K_n}{M_*}}, \quad \mu = \frac{\pi^2 D_n}{8M_*} = \frac{\pi^2}{40n}\sqrt{\frac{K_n}{M_*}}, \tag{10}$$

where the last equality comes from $D_n = 0.2\sqrt{K_n M_*/n^2}$. Note that μ depends on n, but ω does not.

5.2 Numerical model

To confirm these calculations, we perform one dimensional simulations corresponding to the model described above, setting the parameters equal to the two dimensional simulations. We obtain decaying kinetic energy oscillations, as in the two-dimensional case. Extracting the maxima of the oscillations yields curves like those in Fig. 2.

In Fig. 4, we show the kinetic energy oscillation period T for one- and two-dimensional simulations, together with the theoretical prediction π/ω (recall that one period of oscillation in velocity corresponds to two periods in kinetic energy). The oscillation period depends only weakly on n, in accord with the theory. The numerical one-dimensional results converge to the theoretical prediction for large n, probably because the approximation in Eq. (9) is improving. The two-dimensional simulations exhibit longer oscillation periods, probably because the grains are not organized into straight rows.

To measure the decay rate, we fit the oscillation envelopes, such as those shown in Fig. 2 to an exponential:

$$E(t) = E_0 e^{-t/\tau}. \tag{11}$$

The theory predicts $\tau \approx 1/(2\mu)$. The numerical results, together with the theoretical prediction, are shown in Fig. 4. The one-dimensional results agree closely with the theoretical

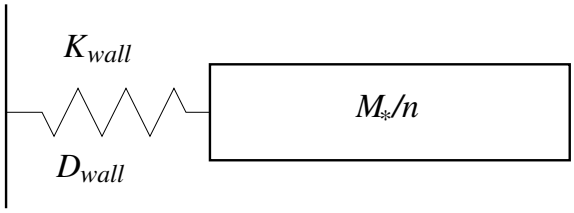

Figure 5: Motivation for soft-wall boundary conditions: We consider the one-dimension chain shown in Fig. 3 as an elastic body attached to the wall by a spring. $K_{\rm wall}$ and $D_{\rm wall}$ are adjusted to maximize energy dissipation.

predictions, but the two-dimensional one are very different. In two-dimensions, $\tau \sim \log n$, as opposed to $\tau \sim n$ in one-dimension. This is a remarkable result, but unfortunately, we do not have space to discuss it here.

6 SOFT BOUNDARIES

There is no reason why the walls must have the same stiffness as the grains. Let us consider the one dimensional system as an elastic body of mass M_*/n connected to the wall with a spring of stiffness $K_{\rm wall}$, as shown in Fig. 5. The mass-spring system has a resonance frequency $\omega_{\rm wall} = \sqrt{nK_{\rm wall}/M_*}$. We adjust $K_{\rm wall}$ so that this frequency is equal to the dominant resonance of the elastic body, so that its vibration energy is transferred to the spring. We then adjust the damping coefficient $D_{\rm wall}$ of the grain-wall interaction to rapidly eliminate this energy. This method has the advantage that it can be implemented by simply modifying the wall-grain interaction. The grain-grain interactions remain unchanged, and the damping occurs mainly at the boundaries, as in the physical system.

More precisely, we choose

$$K_{\rm wall} = K_n/n, \quad D_{\rm wall} = 2\alpha\sqrt{K_n M_*}. \tag{12}$$

The stiffness $K_{\rm wall}$ is chosen so that the resonance frequency in Fig. 5 is equal to the free oscillation frequency studied in Sec. 4. These oscillations should be the longest lived ones, because they have the longest possible wavelength.

The damping $D_{\rm wall}$ is proportional to a constant α whose effect we will study. If we set $\alpha = 1$, the system in Fig. 5 is critically damped.

We now test this method in one- and two-dimensional simulations, obtaining the damping time τ as in Fig. 4. The results are shown in Fig. 6. The damping is indeed very effective. Recall that the oscillation period is about $0.05t_*$, so that $1/\tau \approx 20/t_*$ corresponds to a reduction of amplitude of $1/e$ in one period. Note also that most the values of τ in Fig. 4 correspond to $1/\tau < 1$ in Fig. 6. Therefore, soft walls dramatically increase the damping.

There are some differences between one and two dimensions. The dissipation is slower than in two dimensions. In addition, in two dimensions, $1/\tau$ departs from the approximate

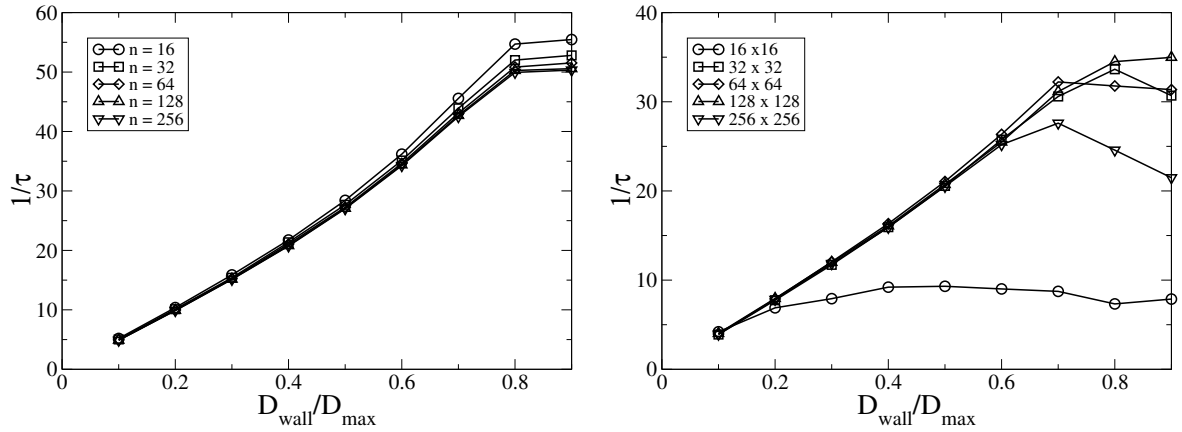

Figure 6: Left: Observed decay rate of the energy in the one-dimensional model, with $K_{\rm wall} = K_n/n$ and $D_{\rm wall}$ given by Eq. (12). Right: The same for two-dimensional simulations, with $K_{\rm wall} = K_n/n$ and $D_{\rm wall}$ given by Eq. (12). Only points with an energy greater than $10^{-16}E_*$ were used to obtain these decay rates.

straight line at high values of $D_{\rm wall}$. There are different causes of this plateau. In the small system ($N = 16\times16$), a single particle is moving to a new equilibrium position. The time needed to find this new equilibrium is long compared to the dissipation time. For large systems, the departure is caused by the appearance at low energies of a complicated oscillation that couples weakly to the boundaries. We believe that these oscillations are not physically relevant. They are strongly damped, and only appear here because the longitudinal oscillations are even more strongly damped.

7 DAMPING OF HIGH FREQUENCY WAVES

To demonstrate the effectiveness of soft wall boundary conditions at higher frequencies, we show in Fig. 7 the response to a delta function external stress $p(t) = p_0\delta(t)$, with $p_0 = 10^{-6}p_*$, applied to the mobile wall. These graphs show the stress on the mobile wall (top lines), on a vertical line of grains in the middle of the domain (middle lines) and on the left fixed wall (bottom line). The pulse introduced at the mobile wall at $t = 0$ can be traced as it travels through the system. At $t \approx 0.0125$, its arrival at the center of the system is signaled by two peaks in the middle curve. This arrival is marked by a circle. At $t \approx 0.025$, its arrival at the left wall is signaled by a deep minimum and marked by another circle. Note that the depth of the minimum is not the same in the two panels: the stress exerted by the soft wall is about half that exerted by the hard wall. This is because the hard wall reverses the motion of the grains, generating a wave that travels back towards the mobile wall, but the soft walls simply stop the grain motion.

When the right wall is hard, the pulse is reflected, and returns back to the mobile wall. It arrives near the middle of the system at $t \approx 0.0375$, and arrives at the mobile wall near $t \approx 0.05$. (Note that this time is very close to the oscillation period of the kinetic energy, as can be seen by examining Fig. 4.) The pulse then reflects off the mobile wall

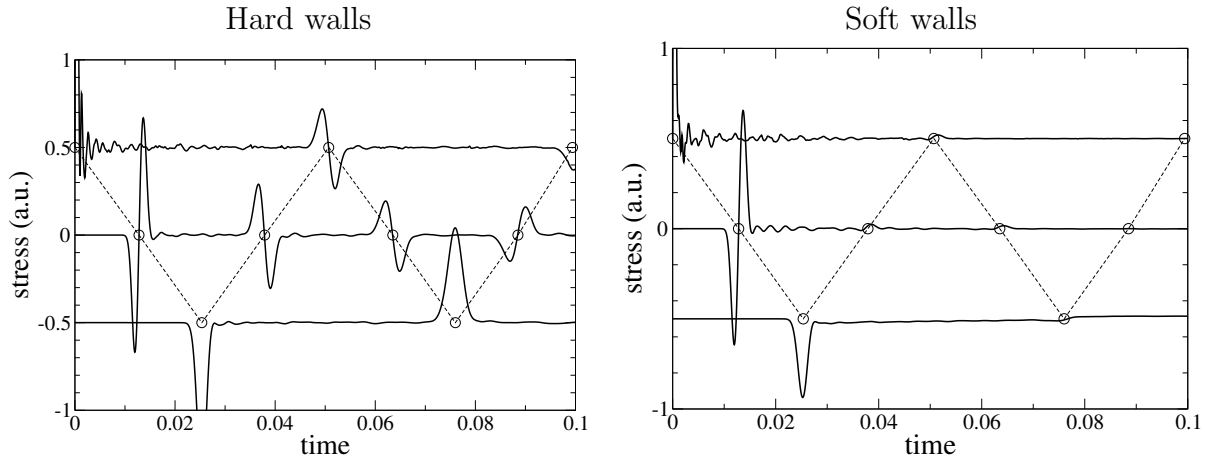

Figure 7: Response to a delta function force applied to the mobile wall. Left: conventional boundary conditions, Right: soft wall boundary conditions. Top curves: stress on the mobile wall. Middle curves: stress on a vertical line of particles near the center of the system. Bottom curves: stress on the left wall. The dotted diagonal lines represent the pulse as it travels back and forth through the system. The cuves are shifted vertically for clarity. Here, the "arbitrary units" are about $10^{-3}p_*$.

and continues its journey. It can be followed for a much longer time than shown above. The pulse gradually spreads, and slowly transforms into a long wave-length standing oscillation, as described by Eq. (6).

When the right wall is soft, the situation is different. The pulse is almost completely absorbed at the right hand wall. Examining the expected arrival times of the pulse (circles) sometimes shows weak disturbances that are close to the noise level. In conclusion, this figure shows that the soft wall boundary conditions act as absorbing boundary conditions.

8 CONCLUSION

The absorbing boundary conditions presented in this paper resemble those used in other fields. The softness of the walls recalls the use of soft, acoustically isolating materials in some experiments. But they also resemble "perfectly matched layers" used in numerical studies of waves in continua. Damping coefficients are made very large just next to the boundary, and this damping is also directionally dependent, for walls exert only normal forces and only normal motions are damped. This means that a wave traveling parallel to a boundary will not (or only weakly) be damped.

This method should open new possibilities for numerical studies of granular acoustics. For example, it should be possible to perform "free space" studies, where the simulation domain represents a small part of an unbounded medium. But open questions remain such as the effect on shear waves.

ACKNOWLEDGMENTS

The author thanks David Imbert for many scientific discussions and for pointing out the existence of Perfectly Matched Layers. This work was supported by ANR (Agence Nationale de la Recherche) project STABINGRAM No: 2010-BLAN-0927-01.

REFERENCES

[1] P.A. Cundall, O.D.L. Strack, A discrete numerical model for granular assemblies *Geotechnique* **29** 47-65 (1979).

[2] J.-P. Berenger, A perfectly matched layer for the absorption of electromagnetic waves, *J. of Computational Physics* **114** 185-200 (1994).

[3] V.A. Bokil, R. Glowinski, An operator splitting scheme with a distributed Lagrange multiplier based fictious domain method for wave propagation problems *J. Comput. Phys.* **205** 242-268 (2005).

[4] O. Mouraille, *Sound propagation in dry granular materials: discrete element simulations, theory, and experiments* Ph.D. Thesis, University of Twente, Enschede, the Netherlands (2009).

[5] S. McNamara, Méthode de Dynamique Moléculaire, in *Modélisation numérique discrète des matériaux granulaires*, p. 25-48, Hermès-Lavoisier (Paris), F. Radjai and F. Dubois, eds. (2010); S. McNamara, Molecular Dynamics Method, in *Discrete-element Modeling of Granular Materials*, p. 1-25, ISTE (London), F. Radjai and F. Dubois, eds. (2011).

[6] V. Yu. Zaitsev, P. Richard, R. Delannay, V. Tournat and V.E. Gusev, Pre-avalanche structural rearrangements in the bulk of granular medium: Experimental evidence *Euro. Phys. Lett.* **83** 64003 (2008)

[7] Y. Khidas, X. Jia, Probing the shear-band formation in granular media with sound waves, *Phys Rev E* **85** 051302 (2012).